PCCP

PAPER

View Article Online
View Journal



Cite this: DOI: 10.1039/c5cp01596k

# Behaviour of NBD-head group labelled phosphatidylethanolamines in POPC bilayers: a molecular dynamics study†

Hugo A. L. Filipe,[abc] Lennon S. Santos,[ad] J. P. Prates Ramalho,[ef] Maria João Moreno[abc] and Luís M. S. Loura*[bcg]

A complete homologous series of fluorescent phosphatidylethanolamines (diC$_n$PE), labelled at the head group with a 7-nitrobenz-2-oxa-1,3-diazo-4-yl(NBD) fluorophore and inserted in 1-palmitoyl, 2-oleoyl-*sn*-glycero-3-phosphocholine (POPC) bilayers, was studied using atomistic molecular dynamics simulations. The longer-chained derivatives of NBD-diC$_n$PE, with $n$ = 14, 16, and 18, are commercially available, and widely used as fluorescent membrane probes. Properties such as location of atomic groups and acyl chain order parameters of both POPC and NBD-diC$_n$PE, fluorophore orientation and hydrogen bonding, membrane electrostatic potential and lateral diffusion were calculated for all derivatives in the series. Most of these probes induce local disordering of POPC acyl chains, which is on the whole counterbalanced by ordering resulting from binding of sodium ions to lipid carbonyl/glycerol oxygen atoms. An exception is found for NBD-diC$_{16}$PE, which displays optimal matching with POPC acyl chain length and induces a slight local ordering of phospholipid acyl chains. Compared to previously studied fatty amines, acyl chain-labelled phosphatidylcholines, and sterols bearing the same fluorescent tag, the chromophore in NBD-diC$_n$PE locates in a similar region of the membrane (near the glycerol backbone/carbonyl region) but adopts a different orientation (with the $NO_2$ group facing the interior of the bilayer). This modification leads to an inverted orientation of the P–N axis in the labelled lipid, which affects the interface properties, such as the membrane electrostatic potential and hydrogen bonding to lipid head group atoms. The implications of this study for the interpretation of the photophysical properties of NBD-diC$_n$PE (complex fluorescence emission kinetics, differences with other NBD lipid probes) are discussed.

Received 19th March 2015,
Accepted 11th May 2015

DOI: 10.1039/c5cp01596k

www.rsc.org/pccp

## Introduction

Biological membranes are fundamental constituents of all cells. Their major function is to define a boundary between the inner and outer cell environments, which is essential for cellular homeostasis.[1–3] Additionally, the involvement of biomembranes in several cellular processes, including energy production, protein synthesis and secretion, signal transduction and cell–cell interactions has been evidenced more recently.[3,4] Among the arsenal of techniques used to study membrane structure and function, fluorescence-based methodologies are most prominent. This role is warranted by the inherent sensitivity of fluorescence (down to single molecule level), coupled with the versatility resulting from the multiplicity of different spectroscopic and imaging fluorescence approaches. Altogether, these features allow the study of important questions in membrane biophysics, such as the extent and kinetics of solute interaction with membranes, lipid trafficking, membrane fusion, location, rotational and translational dynamics, distribution and aggregation state of membrane components and membrane-active molecules.[5]

Because the main structural unit of biomembranes is the phospholipid bilayer, and phospholipids are non-fluorescent, the application of fluorescence approaches to membrane studies requires the use of fluorescent probes. To this effect, designed

[a] Departamento de Química, Faculty of Science and Technnology, University of Coimbra, Largo D. Dinis, Rua Larga, P-3004-535 Coimbra, Portugal
[b] Centro de Química de Coimbra, Largo D. Dinis, Rua Larga, P-3004-535 Coimbra, Portugal
[c] Centro de Neurociências e Biologia Celular, Universidade de Coimbra, Rua Larga, P-3004-504 Coimbra, Portugal
[d] Institute of Chemistry, Federal University of Rio de Janeiro, BR-21941909 Rio De Janeiro, Brazil
[e] Departamento de Química, Escola de Ciências e Tecnologia, Universidade de Évora, Rua Romão Ramalho, 59, P-7000-671 Évora, Portugal
[f] Centro de Química de Évora, Universidade de Évora, Rua Romão Ramalho, 59, P-7000-671 Évora, Portugal
[g] Faculdade de Farmácia, Universidade de Coimbra, Pólo das Ciências da Saúde, Azinhaga de Santa Comba, P-3000-548 Coimbra, Portugal.
E-mail: lloura@ff.uc.pt; Fax: +351 239827126; Tel: +351 239488485

† Electronic supplementary information (ESI) available. See DOI: 10.1039/c5cp01596k

fluorophores with convenient spectroscopic properties, such as absorption and emission in the visible range, high brightness (especially convenient for microscopy and single-molecule techniques), and their sensitivity to the local environment, are frequently used. One such fluorescent group is 7-nitrobenz-2-oxa-1,3-diazol-4-yl (NBD). NBD lipids have been used extensively as fluorescent analogues of native lipids in biological and model membranes to study a variety of processes.[6–8] The photophysical properties of NBD lipids include high fluorescence quantum yield, sensitivity to environment polarity and membrane microviscosity, and suitability for Förster resonance energy transfer (FRET) experiments.

Acyl-chain labelled NBD derivatives are commercially available for all major phospholipid classes. However, it has been shown both experimentally[7,9–12] and by molecular dynamics (MD) simulation[13] that NBD attachment to lipid acyl chains makes the fluorophore prone to loop or ''snorkel'' to the water/lipid interface, due to the chromophore polarity and the acyl chain flexibility. In turn, this effect causes sizeable perturbation of host membrane properties, including considerable loss of cooperativity in the phospholipid main phase transition.[14] Similar effects have also been described for cholesterol analogues labelled with NBD at the alkyl side chain.[15,16]

An obvious way to circumvent this upward looping of the fluorophore is to attach it to the phospholipid head group. To this effect, several NBD head-labelled phosphatidylethanolamine (PE) derivatives are commercially available, including symmetric saturated-chain lipids NBD-di$C_n$PE (1,2-diacyl-*sn*-glycero-3-phosphoethanolamine-*N*-(7-nitro-2-1,3-benzoxadiazol-4-yl)), with acyl chain length $n$ = 14, 16 and 18. NBD-di$C_n$PE probes have been used extensively as model phospholipids in the studies of thermodynamics and kinetics of interaction with lipid bilayers and other hydrophobic aggregates, such as serum lipoproteins.[17–19] Used as FRET donors, NBD-di$C_n$PE probes form, together with acceptor rhodamine B PE derivatives, a very well-known Förster pair for the studies of membrane organization[20–24] as well as quantification of lipid mixing and exchange.[25] Alternatively, NBD probes can be used as acceptors to chromophores including diphenylhexatriene[26,27] or *trans*-parinaric acid,[28] or even as donors and acceptors simultaneously in homo-FRET studies.[20] Several fluorescence spectroscopic and microscopic studies have also indicated that, contrary to the vast majority of membrane fluorescent probes, doubly saturated long-chained NBD-di$C_n$PE partitions favourably to liquid ordered (lo) phases in systems displaying lo/liquid disordered phase coexistence,[22,24,29,30] although the phase preference depends both on the probe acyl chain length and the composition of the underlying lipid mixture.[17,31]

Despite their wide use in membrane biophysics, the behaviour of NBD-di$C_n$PE probes has so far lacked a characterization using MD. Atomistic MD simulations have been recently employed to provide insights into both membrane-inserted probe location, orientation and dynamics and probe-induced host bilayer perturbation (for a review, see ref. 32). Detailed knowledge of NBD preferential location and orientation may help in explaining the particularities of NBD-di$C_n$PE photophysical properties (fluorescence quantum yield, decay and/or anisotropy, orientation of transition dipole in connection to FRET) in comparison with other NBD probes, some of which have been recently characterized by us using MD.[13,16,33] On the other hand, an assessment of the extent of probe-induced perturbation is useful in probe selection for experimental studies. For example, we observed using atomistic MD that fatty amines NBD-$C_n$ are considerably less perturbing than acyl-chain labelled NBD-PC,[14,33] and a small degree of perturbation of fluid phosphatidylcholine (PC) bilayers has been reported for the common FRET acceptor to NBD-di$C_n$PE, rhodamine B PE, also using atomistic MD.[34]

In this article, we study the behaviour of NBD-di$C_n$PE of varying length, $n$ = 4 to 18. We characterize in detail the fluorophore location and orientation, aiming to identify trends among the amphiphiles of this complete homologous series, which may contribute to the improved understanding of the photophysical properties of NBD probes. One intriguing question is to verify whether the NBD fluorophore protrudes into the water phase (similarly to the behaviour reported for rhodamine B PE using atomistic MD[34]) or adopts a similar depth in the bilayer to that of NBD-PC and NBD-$C_n$. In turn, this is expected to influence the degree of probe-induced bilayer perturbation, which will be compared to that of other probes.

## Simulation details

MD simulations and analysis of trajectories were carried out using the GROMACS 4.5.3 package.[35,36] The simple point charge water model was used.[37] The topology of the POPC molecule consisted of a united-atom description for CH, $CH_2$, and $CH_3$ groups, based on the parameters presented by Berger *et al.*[38] for 1,2-dipalmitoyl-*sn*-glycero-3-phosphatidylcholine (DPPC), and by Bachar *et al.*[39] for the oleoyl chain *cis*-double bond. The starting structure was a fully hydrated POPC bilayer (128 POPC:5412 $H_2O$).

The topology of NBD-di$C_{16}$PE was obtained combining the description of DPPC available from Dr D. Peter Tieleman's group webpage[40] with that of the NBD fluorophore, as described in detail by Loura *et al.*[41] Parameterizations of other NBD-di$C_n$PE probes were adapted from NBD-di$C_{16}$PE by adding/removing the appropriate number of methylene groups to/from each chain, for NBD-di$C_{18}$PE or the other probes, respectively. Because NBD-di$C_{16}$PE is anionic at pH close to neutrality,[42] the probes were modelled with global charge −1, with a single hydrogen atom bound to the amine nitrogen. Partial charges of a NBD-di$C_3$PE molecule were derived from *ab initio* quantum mechanical calculations[43] using Gamess-US,[44,45] and used for all studied derivatives. Fig. 1 shows structures and numbering of relevant atoms of the POPC and NBD-di$C_{16}$PE molecules, while the charges adopted for the latter are displayed in Table 1. Bilayers containing NBD-di$C_n$PE molecules (2 in each leaflet) were obtained by randomly inserting probe molecules inside the POPC bilayer without replacement of phospholipids. A corresponding number of $Na^+$ ions were randomly added to the aqueous medium to ensure electroneutrality. In all systems, unfavourable atomic contacts were removed by steepest descent energy minimization. For each system, a short (100 ps) MD run was then carried out using a 1 fs integration step, followed by a 150 ns run using a 2 fs

 

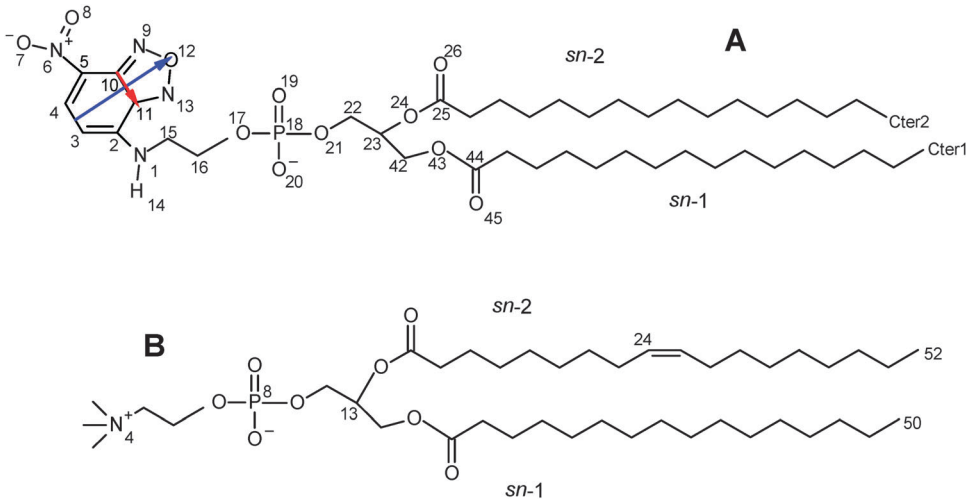


Fig. 1 Structures of NBD-di$C_{16}$PE (A) and POPC (B). The numbering of selected atoms is the same as used throughout the text. The red and blue arrows in (A) define the short and long NBD axes, respectively.

Table 1 Atomic charges used for NBD-di$C_{16}$PE. Identically to the host lipid,[38] acyl-chain $CH_n$ united atoms (unnumbered in Fig. 1A) were modelled with zero charge

| Atom | Charge | Atom | Charge | Atom | Charge | Atom | Charge | Atom | Charge |
|---|---|---|---|---|---|---|---|---|---|
| N1 | −0.20 | O7 | −0.50 | N13 | −0.30 | O19 | −0.77 | C25 | 0.80 |
| C2 | 0.10 | O8 | −0.50 | H14 | 0.30 | O20 | −0.78 | O26 | −0.70 |
| C3 | −0.27 | N9 | −0.30 | C15 | 0.00 | O21 | −0.52 | C42 | 0.23 |
| C4 | 0.28 | C10 | 0.41 | C16 | 0.40 | C22 | 0.30 | O43 | −0.50 |
| C5 | −0.49 | C11 | 0.44 | O17 | −0.54 | C23 | 0.30 | C44 | 0.90 |
| N6 | 1.00 | O12 | 0.03 | P18 | 1.21 | O24 | −0.70 | O45 | −0.63 |

integration step. Bond lengths were constrained to their equilibrium values, using the SETTLE algorithm[46] for water and the LINCS algorithm[47] for all other bonds. All simulations were carried out under constant number of particles, pressure (1 bar) and temperature (298.15 K), and under periodic boundary conditions. Pressure and temperature control were carried out using the weak-coupling Berendsen scheme,[48] and a V-rescale[49] thermostat with coupling times of 1.0 ps and 0.1 ps, respectively. Semiisotropic pressure coupling was used. Van der Waals interactions were cut off at 1.0 nm. Coulomb interactions were calculated using the Particle Mesh Ewald method,[50] with a cut-off of 1.0 nm for the real space component. For visualization of structures and trajectories, Visual Molecular Dynamics software (University of Illinois) was used.[51] The first 50 ns of each simulation were used for equilibration, and the remaining 100 ns were used for analysis.

Deuterium order parameters, $S_{CD}$, were calculated using

$$S_{CD} = (3\langle\cos^2\theta\rangle - 1)/2 \qquad (1)$$

where $\theta$ is the angle between a C–D bond and the bilayer normal, and the brackets denote averaging over time and C–D bonds.[52] In our simulations, using a united atom force field, deuterium positions of acyl chain atoms were constructed from the neighboring carbons assuming ideal geometries. $-S_{CD}$ can vary between 0.5 (full order along the bilayer normal) and −0.25 (full order along the bilayer plane), whereas $S_{CD} = 0$ denotes isotropic orientation.

The electrostatic potential across the bilayer ($z$ coordinate) was calculated by double integration of the charge density:

$$\Delta\psi(z) = \psi(z) - \psi(\infty) = -\frac{1}{\varepsilon_0}\int_z^\infty dz' \int_{z'}^\infty \rho(z'')dz'' \qquad (2)$$

In this calculation, the positions of all atoms were determined relative to the instantaneous centre of mass ($z$ = 0) in all simulations, for each frame. The potential was also averaged and symmetrised for the two bilayer leaflets.[53]

Unless stated otherwise, error estimates were obtained using the block method described by Flyvbjerg and Petersen.[54]

## Results and discussion

### Area per lipid and bilayer thickness

Overall areas per lipid molecule were evaluated by dividing the instant box area by the number of lipid molecules in each monolayer, including those of NBD-di$C_n$PE (66 in total). The time variations in Fig. S1 (ESI†) indicate that equilibration of this parameter is generally achieved after 50 ns. As shown in Fig. S2 (ESI†), after this time the transverse positions of the fluorophores of individual probe molecules across different simulations have also essentially equilibrated. Consequently, as indicated in the preceding section, analysis was carried out considering the last 100 ns of each simulation. The final structures of all simulations are depicted in Fig. S3 (ESI†).

Another aspect which is clear from Fig. S2 (ESI†) is that even the shorter-chained amphiphiles remain inserted in the POPC bilayer at all times, and no molecules were observed to escape to the water medium during simulations. This behaviour agrees with experimental data obtained previously by our group. We measured the lipid/water partition coefficient of NBD-diC$_{14}$PE into POPC bilayers, $K_p = 1.0 \times 10^6$.[17] For a related homologous series (fatty amines NBD-C$_n$), we obtained a linear variation of partition free energy with chain length, with slope $\Delta\Delta G = -(2.4 \pm 0.2)$ kJ mol$^{-1}$.[55,56] From these values, we may extrapolate $\log K_p = 1.6$ for NBD-diC$_4$PE, corresponding to $>95\%$ of bilayer-inserted molecules of this solute (and $>99\%$ of all other amphiphiles of the series) under conditions replicating the setting of our simulations. Still, it is entirely possible that, for much longer simulations, the occasional passage of the shorter amphiphiles to the water phase could be observed.

Fig. 2A depicts the average lipid molecular area $a$ by varying the acyl chain length along the series. The value obtained for pure POPC, $a = (0.66 \pm 0.02)$ nm$^2$, agrees well with published experimental (0.65 nm$^2$, $T = 298$ K;[57] 0.64 nm$^2$, $T = 298$ K;[58] and 0.68 nm$^2$, $T = 303$ K[59]) and simulation (0.655 nm$^2$, $T = 300$ K;[60] 0.68 nm$^2$, $T = 310$ K;[61] 0.652 nm$^2$, $T = 310$ K[62]) reported data. As expected for these diluted systems, the differences between values obtained in the absence and in the presence of different fluorescent probes are not significant. However, a slight overall trend of diminishing $a$ as the chain length increases is noticeable.

PE lipids have smaller head groups than the corresponding PC species, and as such this slight variation could in principle be the simple result of insertion of a molecule with a decreased area per lipid. To ascertain this possibility, we specifically calculated different averages of the areas per POPC and NBD-diC$_n$PE molecules using the APL@Voro software,[63] which carries out a Voronoi tessellation analysis based on selected key atoms (in our case, P atoms of both POPC and NBD-diC$_n$PE). Time variations are displayed in Fig. S4 (ESI†), whereas the time averages of Fig. 2B show that, although in most cases the area per probe is lower than (or identical to, within the statistical uncertainty) the area per POPC molecule, the latter is indeed (even if not significantly so) still reduced in the presence of probe, echoing the overall trend. This is the first indicator that the incorporation of NBD-diC$_n$PE leads to an increase in the bilayer order, especially for the longer chained derivatives. Unsurprisingly, an inverse variation is observed in the variation of the bilayer thickness, calculated as the difference between the average transverse location of the POPC P atoms in the opposing leaflets (Fig. 2A).

### Transverse location and orientation

Fig. 3 shows average locations $\langle z \rangle$ of selected POPC and NBD-diC$_n$PE atoms (see Fig. 1 for numbering) in different probe-inserted systems, relative to the centre of the bilayer ($z = 0$).

The positions of POPC atoms are very similar across all studied systems, and individual differences are mostly within the statistical uncertainty. However, an increasing trend is observed in all atoms, reflecting the above described general decrease in molecular area and increase in bilayer thickness. To some degree, a similar trend is still perceivable in the P18 and C23 atoms of NBD-diC$_n$PE (which correspond to P8 and C13 of POPC, respectively), though considerably blurred by the poorer statistics associated with averaging over 4 molecules instead of 128. The terminal atoms of the probe's acyl chains have, as expected, progressively deeper locations as the chain length is increased. NBD-diC$_{16}$PE is the probe with acyl chains spanning the membrane leaflet most similarly to those of POPC, and its terminal methyl locations match those of the host lipid more closely than any other probe. On the other hand, the acyl chains of NBD-diC$_{18}$PE span the whole leaflet right to the geometrical midplane of the bilayer. Unsurprisingly, a large fraction of configurations show the methyl groups of this probe located beyond this plane, and the fraction of frames for which $z$(Cter) $< 0$ is 53%. This effect is also apparent on the mass density profiles along the bilayer normal, which show (Fig. 4) accumulated density of NBD-diC$_{18}$PE, compared to POPC, close to the bilayer midplane, in addition to the expected density increase in the region corresponding to the fluorophore location for all probes. The similarity between the mass density of the POPC and NBD-diC$_{16}$PE (multiplied by the dilution factor 128/4 = 32) near the centre of the bilayer is remarkable.

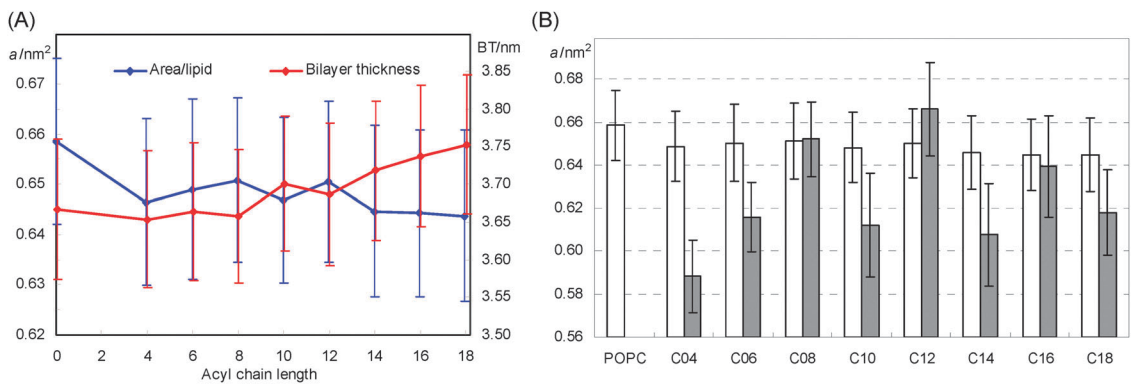


Fig. 2 (A) Average area per lipid $a$ (POPC plus NBD-diC$_n$PE) and bilayer thickness (BT) as a function of NBD-diC$_n$PE acyl chain length. $n = 0$ corresponds to a pure POPC bilayer. (B) Average area per specific lipid components obtained from Voronoi tessellation analysis.[63] White and grey bars denote POPC and NBD-diC$_n$PE, respectively.

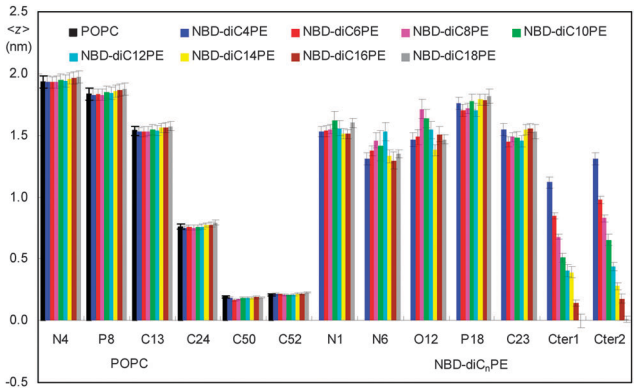


Fig. 3 Average transverse position, $\langle z \rangle$, of specific POPC and NBD-diC$_n$PE atoms in all systems. See Fig. 1 for atom numbering.

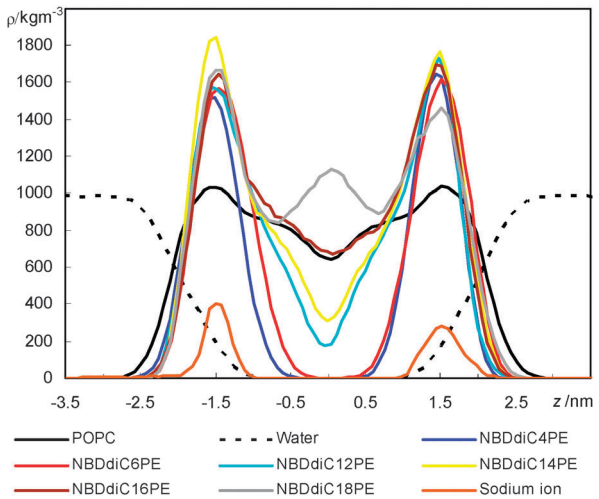


Fig. 4 Mass density profiles across the bilayer normal direction of POPC, solvent, sodium ion (taken from the NBD-diC$_{18}$PE simulation) and selected NBD-diC$_n$PE derivatives. The probe and $Na^+$ curves were multiplied by 32 and 100 (respectively) for better visualisation.

This is in contrast with the previously studied series of fatty amines NBD-C$_n$, in which the alkyl chain is directly attached to the NBD group (instead of having the glycerophosphate linker in between, as in NBD-diC$_n$PE), for which closest behaviour to that of POPC was observed for the C$_{12}$ derivative.[33] Regarding the atoms of the NBD moiety, they are mainly located near the glycerol backbone of POPC (for example, note the similar $\langle z \rangle$ of POPC C13 and NBD-diC$_n$PE N1 atoms), similarly to other NBD probes NBD-C$_n$,[33] NBD-PC,[13] and NBD-cholesterol.[16] However, contrary to these probes, in which the $NO_2$ group was the outermost part of the fluorophore, the amine N1 is generally the most external atom of NBD, located further from the bilayer centre than the nitro N6 atom in all derivatives. This is not surprising given that N1 is also the phosphatidylethanolamine nitrogen atom, and thus part of the labelled lipid head group (corresponding to N4 of POPC). Therefore, linkage of the NBD moiety to a PE lipid leads to an inverted configuration of the fluorophore compared to other NBD probes. Because the overall position of the NBD group is kept closer to the POPC glycerol than to the POPC head group region, another effect of this linkage is that the fluorophore pulls the head group to more internal positions than those observed in POPC. This is most striking in NBD-diC$_n$PE N1, the atom directly involved in fluorophore attachment, which is located (0.40 ± 0.10) nm below POPC N4. Further down the head group, NBD-diC$_n$PE P18 has also a consistently lower $\langle z \rangle$ than POPC P8, and for some of the probes the difference is statistically significant. A minor effect is still observed in NBD-diC$_n$PE C23, compared to POPC C13. Thus, NBD-diC$_n$PE displays a slight inward snorkelling of the head group, in the opposite direction of (and much less pronounced than) the outward snorkelling of the acyl chains of NBD-PC,[13] pulling the phosphoethanolamine group towards the bilayer interior.

### NBD-diC$_n$PE fluorophore and head group orientation

Directly related to the previous discussion is the orientation of the NBD fluorophore in membrane-inserted NBD-diC$_n$PE probes. Fig. 5 shows the angular distributions of the long and short axes of the NBD group, as well as that of the normal to the NBD plane (defined as the vector product of these axes), all relative to the bilayer normal.

Generally, all derivatives have similar angular distributions, and the perceived differences arise mostly from limited sampling due to the small number of probe molecules, no systematic trends being apparent upon varying the acyl chain length. The long axis (Fig. 5A) has bimodal angular distribution, meaning that it can either point to the direction of the water or to that of the bilayer centre. The short axis of the NBD fluorophore has a very broad angular distribution (Fig. 5B), centred between 60° and 90° relative to the bilayer normal, implying that the $NO_2$ group has an almost perpendicular orientation relative to the bilayer normal (pointing slightly inwards, in contrast with NBD-C$_n$,[33] NBD-PC,[13,64] and NBD-cholesterol,[16] where, as mentioned above, it points clearly to the water medium). The normal to the NBD plane (Fig. 5C) is mostly oriented perpendicularly to the bilayer normal.

Fig. 5D shows the orientation of the P–N axis of both POPC in pure bilayers and NBD-diC$_n$PE in the systems containing probe molecules. For POPC, the average tilt of this vector relative to the bilayer normal is (77 ± 2)°, indicating an orientation roughly along the membrane plane (with the choline group in a slightly more external position, as already seen in the transverse positions of N4 and P8, shown in Fig. 3). This value is in excellent agreement with that reported by Gurtovenko and Vattulainen (78°) for POPC at 310 K.[62,65] For the probes, average tilts at around 120° are obtained (they vary without noticeable trends between 110° for NBD-diC$_{12}$PE and 136° for NBD-diC$_{14}$PE), indicating a more inward location of the NBD-diC$_n$PE N1 atom (which is the corresponding atom of N4 in POPC) compared to P18. This inverted head group configuration is not seen in acyl chain NBD-labelled phospholipids C6-NBD-PC and C12-NBD-PC, for which no discernible differences in P–N angular distributions were observed compared to pure PC.[14] Many of the molecules illustrated in the snapshots of Fig. S3 (ESI†) adopt the

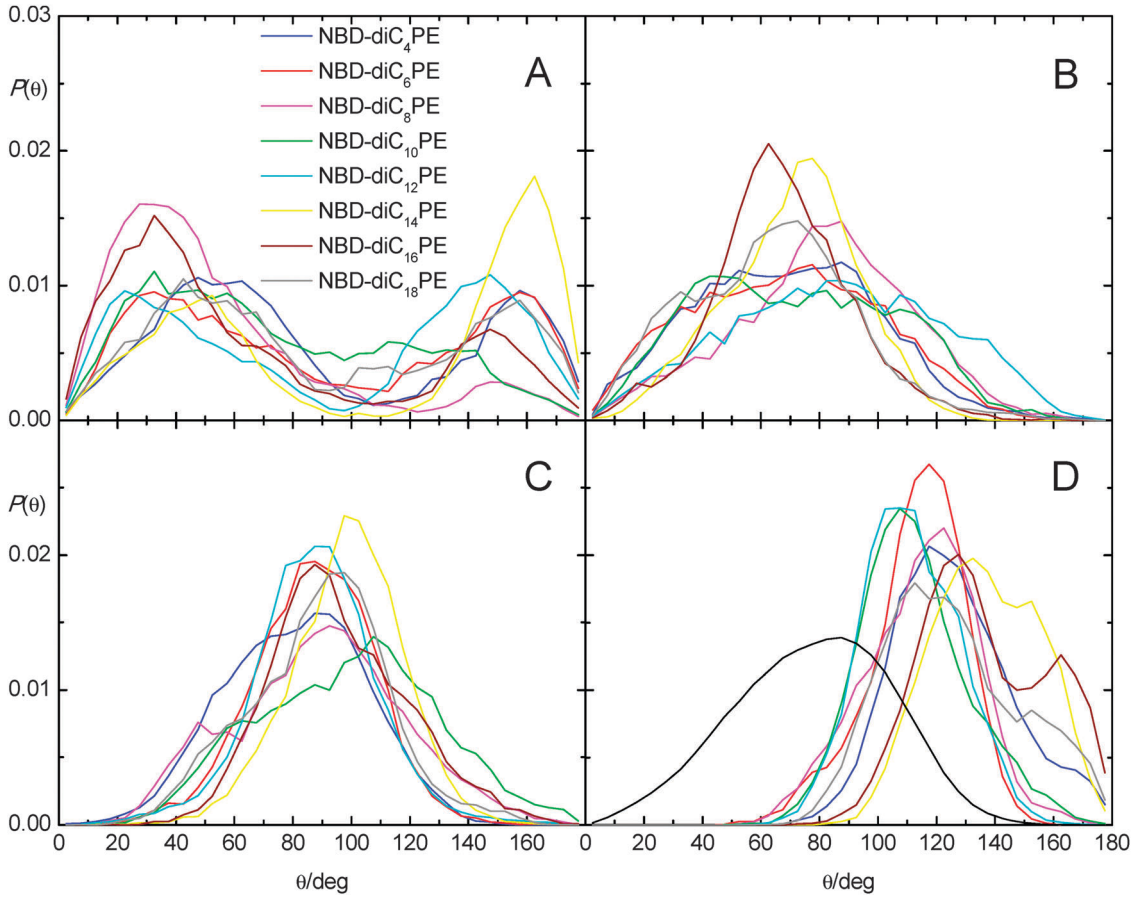


Fig. 5 Angular orientation distributions for the long (A) and short (B) axes of the NBD fluorophore, normal to the NBD group (C), as well as for the P–N axes (D) of NBD-diC$_n$PE (P18–N1) and POPC (P8–N4, smooth black line), all relative to the bilayer normal. For numbering and definition of NBD axes, see Fig. 1.

corresponding "inverted snorkelling" configurations of the NBD fluorophore.

### Hydrogen bonding

In previous studies of related NBD-bearing probes in phospholipid bilayers, hydrogen bonds, either involving the NBD N1H14 group as a donor to water or lipid atoms, or water OH donor groups to NBD N and O atoms, were identified as persistent interactions, crucial for the placement of the fluorophore in the carbonyl/glycerol region.[13,16,33] To verify whether this also applies to NBD-diC$_n$PE, we studied the occurrence of H-bonds featuring probe atoms either as donors (Fig. 6A) or as acceptors (Fig. 6B). For this purpose, an H-bond for a given donor–H–acceptor triad was registered each time the donor–acceptor distance was less than 0.35 nm and the H–donor–acceptor angle was $<60^{\circ}$.

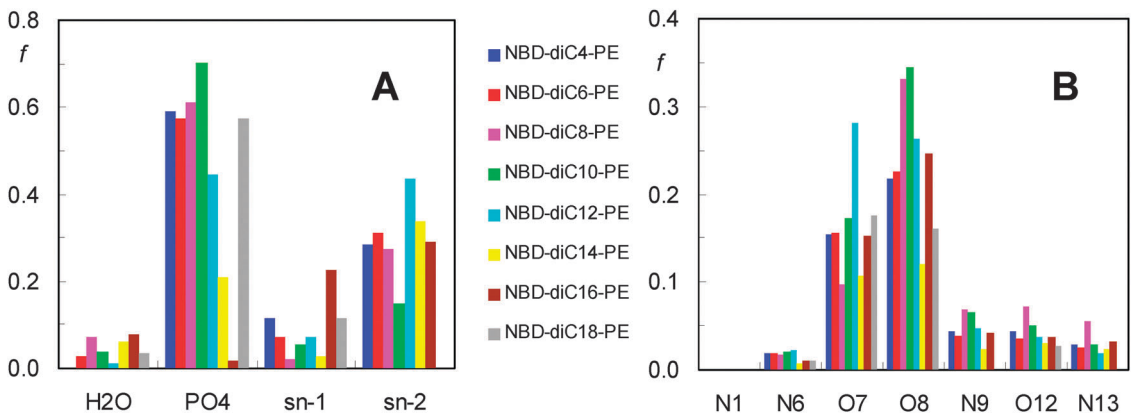


Fig. 6 H-bond fractional frequencies ($f$) of the NBD N1–H14 donor to POPC or water acceptor atoms (A) and of the water donor to NBD acceptor atoms (B).

Fig. 6A shows that the NBD N1H14 group is almost permanently involved as a H-bond donor to other atoms, as the sum of fraction of simulation time $f$ across the possible acceptor atoms (water and POPC O atoms) is close to unity for all derivatives. This generally occurs most frequently with phosphate O atoms, at variance with NBD-$C_n$,[33] C12-NBD-PC,[13] and 22-NBD-cholesterol,[16] for which phospholipid ester O atoms are the main acceptors. This difference between NBD-di$C_n$PE and the other NBD probes probably stems from the more external location of the N1–H14 group, which favours interactions with head group O acceptors over those in the glycerol/carbonyl region. A significant fraction of H-bonds still occurs for O atoms at the top of the *sn*-2 chain (slightly more external than those at the top of the *sn*-1 one; see Fig. 1 for definition of *sn*-1 and *sn*-2 chains), similarly to NBD-$C_n$ and C12-NBD-PC. The two derivatives which presented higher fractions of H-bonding to ester/carbonyl rather than phosphate atoms were NBD-di$C_{14}$PE and NBD-di$C_{16}$PE, which are also those that display deeper transverse location of the N1 atom (Fig. 3). This indicates that slight differences in depth of this donor atom correspond to sizeable variations in its pattern of H-bonding interactions. On the other hand, Fig. 6B shows that NBD N and O atoms are frequently involved as acceptors in H-bonding interactions with water, especially the most electronegative O atoms of the $NO_2$ group. This behaviour is identical to that observed in other NBD probes.[13,16,33]

### Order parameters

Deuterium order parameters, $S_{CD}$, as defined by eqn (1), are obtained experimentally from deuterium NMR quadrupole splittings in membranes made up of deuterated phospholipids, and may be calculated readily from MD simulations (see Simulation details). They constitute a measure of the orientational mobility of lipid acyl chains.[52,66] In liquid crystalline bilayers, $-S_{CD}$ profiles along a saturated acyl chain (such as POPC *sn*-1) have a characteristic shape, showing relatively small variation between the C2 and C8 atoms, and decreasing markedly for more internal positions. For the POPC *sn*-2 monounsaturated chain, a characteristic dip is found near the middle, corresponding to the distinct conformation around the double bond. Perturbation resulting from incorporation of solutes such as probe molecules may lead to increased or decreased membrane order, and correspondingly higher or lower order parameter profiles (respectively), compared to the host lipid.

Fig. 7 shows $-S_{CD}$ for the chain C atoms of the different probes of the series, whereas Fig. 8 depicts the overall $-S_{CD}$ profiles of POPC in the different systems. For pure POPC, the results agree closely with both experimental (*e.g.*, ref. 67–69) and simulation (*e.g.*, ref. 60, 62 and 67) published profiles.

As expected, the order parameter decreases along the chain for each fluorescent derivative, pointing to an increased fraction of *gauche* conformers as the end of the chain is approached. Additionally, in most of the cases, $-S_{CD}$ increases with the chain length when comparing the values calculated for the different probes at a given position along the chain, especially in the case of the *sn*-1 chains, which most closely resemble those of POPC. This is expected, because the longer the chain, the stronger is its anchoring effect in the bilayer for corresponding positions along the former. In particular, the shorter chained derivatives NBD-di$C_4$PE and NBD-di$C_6$PE can only penetrate the bilayer shallowly (as visually evidenced in Fig. S3B and S3C, ESI†), and hence their $-S_{CD}$ values are the lowest among the series. Despite the obvious fact that the probe curves are affected by the limited averaging provided by the four NBD-di$C_n$PE molecules, it is noteworthy that the *sn*-1 $-S_{CD}$ profiles of the longer derivatives resemble most to that of POPC (Fig. 8A).

On the other hand, both panels of Fig. 8 indicate that the POPC order parameters show a slight increase upon increasing probe chain length $n$, in accordance with the area/lipid and bilayer thickness results. Overall, this effect is not very pronounced, which is again justified by the low probe mole fraction. However, this does not rule out the existence of a stronger local effect, which may be especially relevant for fluorescent probes, given that they can only report on their immediate surroundings. To check whether this scenario applies to the NBD-di$C_n$PE family, we calculated $-S_{CD}$ for varying lateral distance $R$ to the closest probe molecule in the same bilayer leaflet. Fig. 9 depicts averages over the whole *sn*-1 chains, obtained for different ranges of $R$ values. The corresponding detailed profiles are given in Fig. S5 (ESI†).

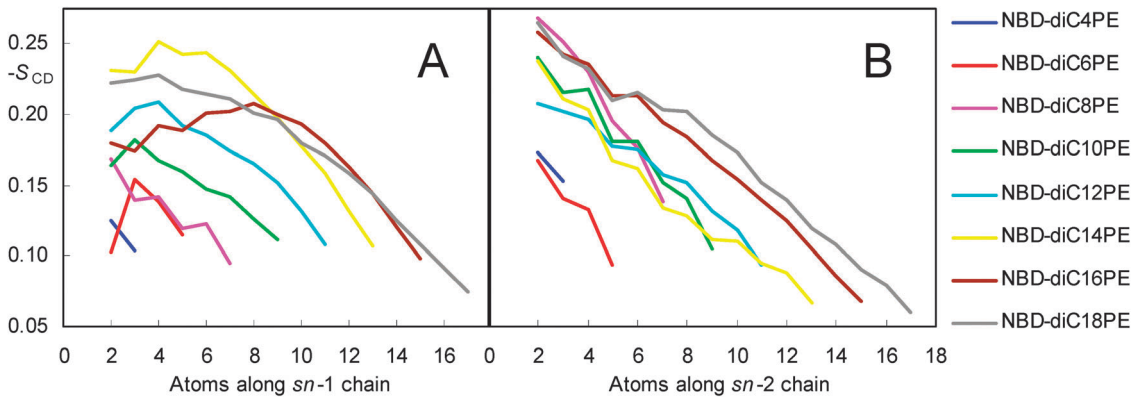


Fig. 7 Deuterium order parameter of the NBD-di$C_n$PE probes, as a function of the *sn*-1 (A) or *sn*-2 (B) acyl chain carbon segment.

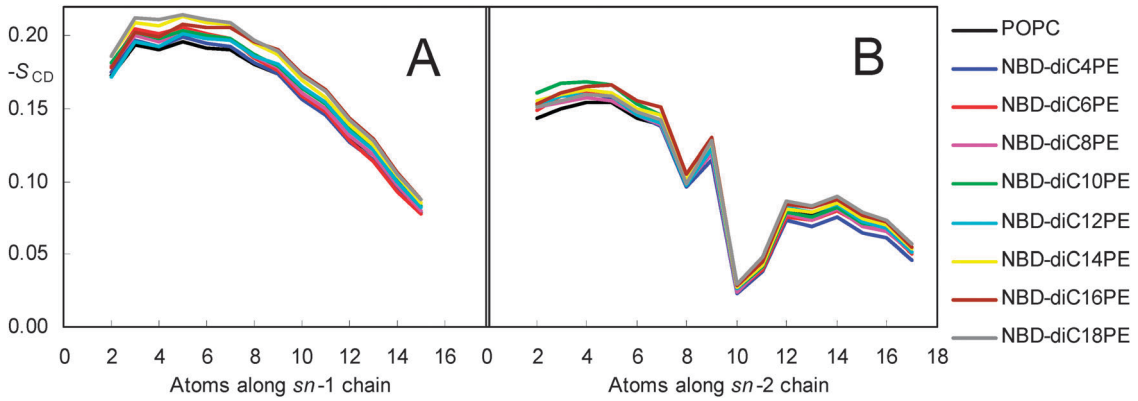


Fig. 8 Deuterium order parameter of POPC, in the absence and in the presence of NBD-diC$_n$PE probes, as a function of the *sn*-1 (A) or *sn*-2 (B) acyl chain carbon segment.

It is observed that POPC molecules in close vicinity ($R < 0.4$ nm) of NBD-diC$_{16}$PE are indeed more ordered than those in the absence of probe (see Fig. 9 and Fig. S5G, ESI†), but this effect is modest (note that uncertainty in this calculation is relatively high, because of the reduced number of lipid chains in this situation). Moreover, for all other derivatives, average order parameters are lower for POPC chains adjacent to NBD-diC$_n$PE, especially for $n \leq 10$. Shorter probe acyl chains lead to the appearance of voids underneath the terminal methyl groups. Filling of this free space with nearby lipid acyl chains implies tilting of the latter and reduction in their order parameter. Conversely, chains that are longer than the lipid hydrophobic length may induce local readjustments of the adjacent lipid acyl chains, possibly leading to reduced order parameter values compared to the case of ideal matching. A similar situation has been experimentally described for homologous series of sterols with branched[70] or linear[71] aliphatic chains, for which maximal ordering effects are found for an intermediate chain length.

Thus, the data of Fig. 9 and Fig. S5 (ESI†) indicate that there is a general overall increase of POPC order parameters despite the fact that, in most cases, NBD-diC$_n$PE causes decrease of this parameter for nearby lipid acyl chains. In numerical terms, this apparently puzzling result stems from the fact that $-S_{CD}$ of the second-neighbouring (0.4 nm $< R <$ 0.8 nm) and bulk POPC chains ($R >$ 0.8 nm) is increased compared to pure POPC. Because there are considerably more POPC chains in these more distant $R$ value ranges, overall averages tend to be slightly (consistently for all probes except NBD-diC$_4$PE, but within the statistical uncertainty for $n < 14$) higher for probe-loaded bilayers than for pure lipid. In physical terms, this result excludes the possibility of the inserted anionic probes being the main responsible species for the overall membrane ordering in most systems. Superficially, this observation seems at odds with MD simulation studies of mixed membranes containing zwitterionic PC and anionic phosphatidylserine (PS) lipids, which revealed that the latter induced lateral bilayer condensation,[72,73] to average area/lipid values lower than calculated from linear combination of the values obtained for each component in the corresponding pure system (weighted by the respective mole fraction).[73] In these PC–PS mixtures, this phenomenon may partly result from H-bonding interactions involving PS NH donors and PC oxygen acceptor atoms.[72,73] Similarly to PS, NBD-diC$_n$PE have a NH group, which is capable of acting as a H donor to PC oxygen atoms (Fig. 6A). However, in terms of lipid chain order of POPC/NBD-diC$_n$PE systems, this potentially ordering interaction is counterbalanced by (i) the bulky nature of the NBD fluorophore, which renders the head group of NBD-diC$_n$PE much larger than that of PS (the one that López Cascales *et al.*[73] obtained has an area/lipid value of pure PS $\sim$0.15 nm$^2$ lower than that of pure PC. Judging from the Voronoi tessellation areas of Fig. 2B, much smaller differences between the zwitterionic and anionic lipids exist in our systems); and (ii) the above mentioned hydrophobic mismatch between POPC and NBD-diC$_n$PE (NBD-diC$_{16}$PE, the sole probe that displays hydrophobic matching with POPC, is the only one capable of inducing local host lipid acyl chain ordering).

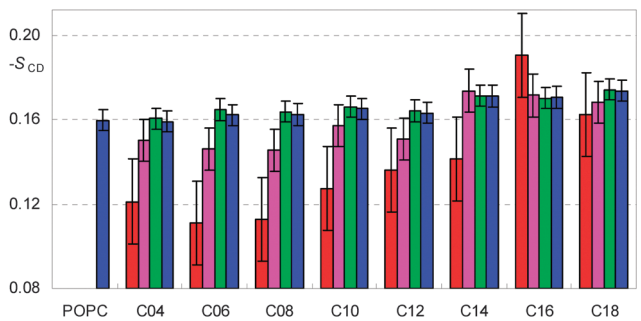


Fig. 9 Average (over all atoms between C2 and C15) order parameter of the POPC *sn*-1 chain as a function of the lateral distance $R$ to the closest NBD-diC$_n$PE molecule in the same bilayer leaflet. Red, magenta, green and blue bars denote $R < 0.4$ nm, 0.4 nm $< R <$ 0.8 nm, $R >$ 0.8 nm, and overall average, respectively.

Therefore, if an overall order increase exists despite local disordering by anionic NBD-diC$_n$PE, it must stem from the other added component, $Na^+$. Increases in the order of POPC acyl chains in the presence of NaCl have been described both experimentally[74] and by MD simulations.[60,62,75] These MD studies showed that the chloride ion has an external distribution, with a maximum clearly outside that of the POPC head group atoms, and probably has little if any impact on acyl

chain order. On the other hand, and similarly to the present study (Fig. 4), these literature studies demonstrated that sodium penetrates well inside the head groups, and interacts strongly with glycerol/carbonyl lipid atoms. We have also found very strong specific interactions of $Na^+$ with these atoms in both POPC and NBD-di$C_n$PE, as illustrated in the radial distribution function plots of Fig. S6 (ESI†), which display well-defined peaks (the first at $R \sim 0.21$–$0.22$ nm). A preferential association of $Na^+$ with *sn*-2 ester atoms (compared to *sn*-1) is consistently verified for POPC in all systems (and for probes in most of them, including NBD-di$C_{18}$PE as shown in Fig. S6, ESI†), probably resulting from the more external location of the O atoms in the *sn*-2 chain, as well as their more electronegative character in the parameterization used here.[38] In any case, clear preference for ester relative to phosphate (in both POPC and probe) and electronegative atoms of the NBD fluorophore is observed. Due to the position of these ester O atoms at the top of the acyl chains, binding of sodium is very likely a cause of increased order in this region of the bilayer, which propagates to the lower chain segments. This effect supersedes the local probe-induced disordering in all systems, with the sole exception of NBD-di$C_4$PE. Curiously, one can observe similar effects (local disordering, but increased overall order parameter) on the MD simulation results of anionic Texas Red-di$C_{16}$PE with $Na^+$ counterions,[76] which suggests that this may be a relatively common pattern for anionic membrane-inserted solutes with sodium counterions. In fact, even in PC–PS mixtures, bridging of lipid molecules by $NH_4^+$ or $Na^+$ counterions was demonstrated as an additional cause of interlipid complexation and bilayer condensation.[72,73] It would be interesting to investigate whether replacement of $Na^+$ with $K^+$ (which binds to lipid oxygen atoms much more weakly[62]) leads to significant differences.

### Electrostatic potential

In previous reports, we showed that incorporation of NBD-PC[14] and NBD-$C_n$[33] causes an increase in the electrostatic potential difference between the bilayer and water phases. NBD-di$C_n$PE presents two differences compared to these probes: the different configuration of the NBD fluorophore and the P–N dipole (the latter compared only to NBD-PC, as this dipole is absent in NBD-$C_n$); and their ionized state (whereas NBD-PC and NBD-$C_n$ were globally uncharged, NBD-di$C_n$PE is anionic at neutral pH, and electroneutrality is maintained by the addition of sodium ions).

As shown in Fig. 10A, inclusion of NBD-di$C_n$PE probes increases the difference in the electrostatic potential between the interior of the bilayer and bulk water. These values are subject to uncertainty due to cancellation errors, because the observed potential profile is the summation of water, lipid, probe, and ionic contributions, which almost cancel each other (Fig. 10B). Still, the added contribution of the NBD-di$C_n$PE and its counter ions $Na^+$ to $\Delta\psi(0)$ is positive, unlike that of the unlabeled phospholipid, as seen more clearly in Fig. 10C. This situation is reminiscent of that found for POPC bilayers in the presence of NaCl, where the distributions of the cations (near the carbonyl/glycerol region) and anions (displaced into the water phase) set up a capacitor that induces a considerable electric field in the head group region and an overall increase in the water/bilayer electrostatic potential difference.[60,62] Here, instead of residing

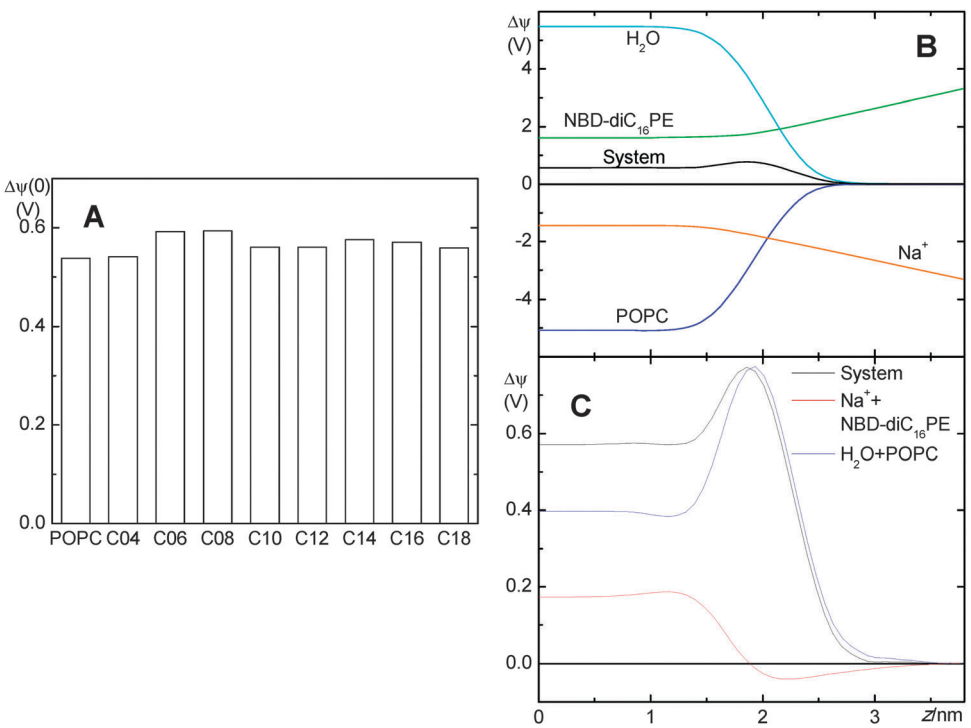


Fig. 10 (A) Electrostatic potential difference between the bilayer centre and the bulk water phase for all systems. (B, C) Overall profile and individual contributions to the electrostatic potential.

in the chloride atoms, the anionic charge is located in the lipid head groups, but it is still distributed more externally than the cationic charge, and the overall effect is similar.

### Lateral diffusion

Lateral diffusion coefficients $D$ were calculated from the two-dimensional mean squared displacement (MSD), using the Einstein relation

$$D = \frac{1}{4}\lim_{t\to\infty}\frac{\mathrm{dMSD}(t)}{\mathrm{d}t} \quad (3)$$

In turn, MSD is defined by

$$\mathrm{MSD}(t) = \langle\|\vec{r}_i(t + t_0) - \vec{r}_i(t_0)\|^2\rangle \quad (4)$$

where $\vec{r}$ is the $(x,y)$ position of the centre of mass of molecule i of a given species, and the averaging is carried out over all molecules of this kind and time origins $t_0$. To eliminate noise due to fluctuations in the centre of mass of each monolayer, all MSD analyses were carried out using trajectories with a fixed centre of mass of one of the monolayers, and the final result is averaged over the two leaflets. Fig. S7 (ESI†) shows MSD for NBD-diC$_n$PE and POPC, while the corresponding $D$ values (obtained from fits to the linear region of the MSD plots) are given in Fig. 11.

The diffusion coefficient of POPC in the pure system ($D$ = $(3.3 \pm 0.2) \times 10^{-8}$ cm$^2$ s$^{-1}$) agrees well with values obtained both from NMR experiments ($D = (4.0 \pm 0.8) \times 10^{-8}$ cm$^2$ s$^{-1}$)[77] and MD simulations ($D = (3.9 \pm 0.3) \times 10^{-8}$ cm$^2$ s$^{-1}$)[60] near room temperature. Although the changes upon insertion of NBD-diC$_n$PE are minor and inside the statistical uncertainty, it appears that POPC $D$ is slightly lower for the systems with longer probe acyl chains, possibly reflecting the increasingly ordered bilayers. Compared to the host lipid, probe diffusion is generally slower, which can be explained on account of the interactions between the NBD group and both the solvent and the host lipid (the fluorophore of NBD-diC$_n$PE is effectively replacing the choline group of PC, which is incapable of hydrogen bonding). Overall, there are no established trends of variation of lateral diffusion coefficients with increasing chain length, in agreement with the FRAP measurements of Vaz *et al.*[78] The two possibly variant results are the calculated higher value of NBD-diC$_{10}$PE and the lower value of NBD-diC$_{18}$PE. Although both could be regarded as outliers stemming from the small number of probe molecules sampled (the shapes of the respective MSD curves seem to differ from those of the other derivatives), it is possible that an increased $D$ value for intermediate chain length results as a compromise between two opposing effects: on the one hand, the increased order of the bilayer for longer chains, which would *per se* lead to a continuous decrease in $D$; on the other hand, the increasing weight of the acyl chain atoms (which are located in a more fluid region of the bilayer, and therefore more capable of short-range segmental motions that are taken into account in our MSD calculation). Ultimately, the increase in order prevails for the very long chains of NBD-diC$_{18}$PE, which has the lowest $D$ value. In this latter result, partial interdigitation of probe acyl chains into the opposing leaflet may also play a role in the slower lateral diffusion, as found in the NBD-C$_n$ series.[33]

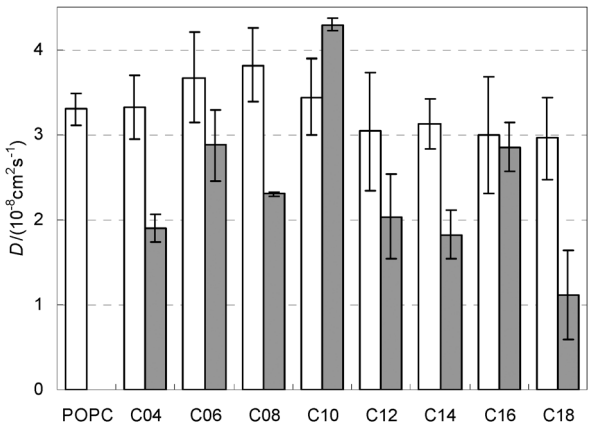


Fig. 11 Lateral diffusion coefficients $D$ of POPC (white bars) and NBD-diC$_n$PE (grey bars).

### Relation to photophysical properties

The use of head group-conjugated phosphatidylethanolamines as fluorescent membrane probes is very common in membrane biophysics.[79] While it is tempting to believe that by attaching a fluorescent tag to this part of a phospholipid molecule one ensures a convenient location of the fluorophore in this region, avoiding perturbation of the membrane glycerol backbone and the hydrocarbon core, results obtained by different techniques have pointed that this is not necessarily the case. MD simulations of Texas Red-diC$_{16}$PE have suggested that this fluorophore, despite its polarity and sheer size, bends towards the centre and penetrates inside the apolar region of DPPC fluid vesicles.[76,80] For NBD-diC$_n$PE, in particular, fluorescence quenching studies have indicated conflicting transverse locations. Using the parallax method, Chattopadhyay and London reported a transverse distance $z$ = 1.42 nm between the fluorophore of NBD-diC$_{16}$PE and the centre of DOPC membranes,[9] which was later revised to the considerably more external values $z$ = 1.89 nm[10] and 2.03 nm,[81] obtained with different combinations of spin-labelled quenchers. These large differences cast important doubts about the reliability of parallax quenching depth determinations, which assume drastic approximations, such as purely static quenching and precise transverse location of two reference quenchers (which must be accurately known), and uses large membrane concentrations of the latter (typically 10 mol%). The present MD study indicates a fluorophore location of around $\sim$1.4 nm relative to the centre of POPC membranes, therefore in close agreement with the earliest quenching determination. In accordance with all quenching studies, the locations determined by us for both NBD-diC$_n$PE and NBD-PC[13] are very similar (see full discussion below). For NBD-PC in particular, this MD-derived location near the glycerol backbone/carbonyl region agreed with NMR cross-relaxation rate measurements,[11] which gives us confidence regarding the NBD-diC$_n$PE position determined here with essentially identical simulation parameters.

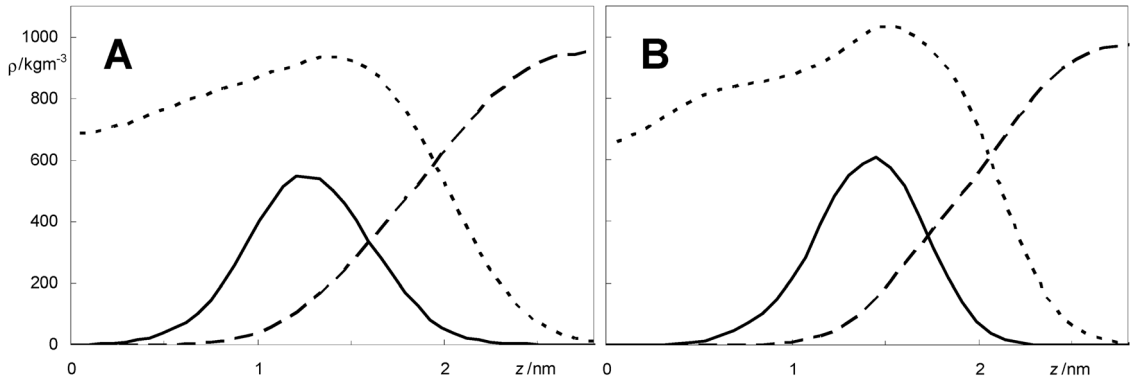


Fig. 12 Mass distributions of the NBD fluorophore (solid line; multiplied by the dilution factors 128/4 = 32 (A) or 64/4 = 16 (B) for better visualisation), water (dashed line) and the host lipid (dotted line) in the (A) C6-NBD-PC/DPPC[13] and (B) NBD-diC$_{16}$PE/POPC systems.

A similar location of the fluorophore in bilayer-inserted NBD-PC and NBD-diC$_n$PE is consistent with the almost coincident maximal absorption and emission wavelengths of the two probes,[7] both close to those found for the NBD fluorophore in medium-polarity solvents such as ethanol or acetonitrile.[82] At this point, it is useful to compare the location and solvent accessibility of the NBD fluorophore (taken as atoms 1–14 in Fig. 1) in the present study with our previous investigation of NBD-PC in fluid DPPC (323 K).[13] Fig. 12 depicts the mass distribution of NBD in the C6-NBD-PC/DPPC and NBD-diC$_{16}$PE/POPC systems, while values of relevant parameters are listed in Table 2.

It is clear that the systems are not equivalent, and the fluid DPPC bilayer is thinner by $\sim$0.3 nm compared to that of POPC. Comparing the respective locations of lipid atoms N4, P8 and C13, this difference should correspond to a $\sim$0.12 nm depth variation in the region where NBD is preferentially located. From the densities $\rho$ of water and NBD, one can calculate the average mass density of solvent sensed by the fluorophore. This metric of polarity was introduced by us in a recent MD study of pyrene-labelled membranes:[83]

$$\langle \rho(\text{water}) \rangle_{\text{fluorophore}} = \frac{\int \rho_{\text{fluorophore}}(z)\rho_{\text{water}}(z)\mathrm{d}z}{\int \rho_{\text{fluorophore}}(z)\mathrm{d}z} \qquad (5)$$

Altogether, the data of Table 2 indicate that the fluorophore average locations and water accessibilities are largely identical for NBD-diC$_n$PE and NBD-PC. On close inspection of Fig. 12, one finds that, despite the transversally compressed system, the NBD mass distribution is slightly wider in NBD-PC than in NBD-diC$_n$PE. This may be quantified by calculating the standard deviation of transverse location distribution:

$$\sigma_z = \sqrt{\int (z - \langle z \rangle)^2 \rho_{\text{fluorophore}}(z)\mathrm{d}z \Big/ \int \rho_{\text{fluorophore}}(z)\mathrm{d}z} \qquad (6)$$

where the average distribution value $\langle z \rangle$ is calculated according to

$$\langle z \rangle = \int z\rho_{\text{fluorophore}}(z)\mathrm{d}z \Big/ \int \rho_{\text{fluorophore}}(z)\mathrm{d}z \qquad (7)$$

As shown in Table 2, $\sigma_z$ is higher by $\sim$14% in the C6-NBD-PC/DPPC system, compared to NBD-diC$_{16}$PE/POPC. However, this difference is probably not significant. The depth range $[\langle z \rangle - 2\sigma_z, \langle z \rangle + 2\sigma_z]$, inside which there is $\sim$96% probability of finding the fluorophore (for normal distributions; from the shape of the actual curves, this is a reasonable approximation) is [0.60 nm, 1.95 nm] for C6-NBD-PC/DPPC and [0.81 nm, 1.99 nm] for NBD-diC$_{16}$PE/POPC, corresponding to 3.5 kg m$^{-3}$ < $\rho_{\text{water}}(z)$ < 600 kg m$^{-3}$ and 1.2 kg m$^{-3}$ < $\rho_{\text{water}}(z)$ < 555 kg m$^{-3}$ ranges of water density, respectively.

These are small differences, and the most important result is that both probes have very wide transverse distributions. This is probably the main reason for the decay heterogeneity most often found in the fluorescence decays of NBD lipid analogues. Whereas the decay of *N*-propylamino NBD (NBD-C$_3$) emission may be described by a single exponential function in a variety of pure solvents,[82] the huge possible variations in environment polarity that may be experienced by membrane-inserted fluorophores of NBD-PC and NBD-diC$_n$PE dictated otherwise. For example, in fluid DPPC vesicles (50 °C) with 0.1 mol% NBD lipid, both NBD-diC$_{16}$PE ($\tau_1$ = 0.87 ns (25% pre-exponential), $\tau_2$ = 6.61 ns (75%), intensity-weighted average lifetime $\langle \tau \rangle$ = 6.37 ns[20]) and C6-NBD-PC ($\tau_1$ = 0.94 ns (20%), $\tau_2$ = 6.16 ns (80%), $\langle \tau \rangle$ = 5.97 ns[27]) present bi-exponential decays, with similar contributions of a short lifetime component, close to that measured for NBD-C$_3$ in water (1.0 ns).[82] Similarly heterogeneous decays were measured in other lipid systems.[81,84] These complex decays would probably be more correctly described

Table 2 Comparison of transverse positions of selected lipid atoms, NBD distribution parameters, and NBD-averaged water density in the C6-NBD-PC/DPPC[13] and NBD-diC$_{16}$PE/POPC systems

| | C6-NBD-PC/DPPC | NBD-diC$_{16}$PE/POPC |
|---|---|---|
| $\langle z \rangle$(host lipid N4)/nm | 1.81 ± 0.04 | 1.96 ± 0.05 |
| $\langle z \rangle$(host lipid P8)/nm | 1.73 ± 0.04 | 1.87 ± 0.05 |
| $\langle z \rangle$(host lipid C13)/nm | 1.44 ± 0.04 | 1.57 ± 0.04 |
| maximum of NBD distribution/nm | 1.21 | 1.45 |
| $\langle z \rangle$ of NBD distribution/nm | 1.28 | 1.40 |
| $\sigma$ of NBD distribution/nm | 0.34 | 0.30 |
| $\langle \rho_{(\text{water})} \rangle_{\text{NBD}}$/kg m$^{-3}$ | 183 | 172 |

by continuous unimodal lifetime distributions,[85] because the transverse location distributions of NBD are, in fact, wide, single-peak curves.

In the experimental fluorescence studies on bilayers mentioned above, it was consistently found that the decay of NBD-diC$_n$PE emission is somewhat slower than that of C6-NBD-PC (with that of C12-NBD-PC being slightly faster than the latter). We could not clarify the precise origin of this effect, but it is most probably related to properties other than the transverse location. In NBD-PC, the fluorophore preferably adopts configurations pointing the $NO_2$ group to the water phase, whereas in NBD-diC$_n$PE it is almost oriented perpendicular to the bilayer normal (pointing slightly inwards). In NBD-PC, the amino NH group acts as a H-bond donor mostly to lipid carbonyl and ester O atoms, whereas in NBD-diC$_n$PE the most frequent H-bond acceptors are lipid phosphate O atoms. These differences in orientation and specific interactions with lipid atoms (not water atoms, as the H-bonding from water occurs equally often and to the same NBD atoms as in other analogues) are probably related to the distinct emission properties of NBD-diC$_n$PE.

The NBD transition dipole (parallel to the NBD short axis[13,86]) has different orientation in NBD-diC$_n$PE compared to NBD-PC. As commented above, whereas the nitro group of NBD-PC is pointed towards the water phase, that of NBD-diC$_n$PE shows inward orientation (for a direct comparison of the angular distributions of the NBD long and short axes in NBD-PC and NBD-diC$_{16}$PE, see Fig. S8, ESI†). This also bears consequences for the quantification of FRET rates and efficiencies in experiments involving this probe. We recently developed a simple numerical simulation method for the estimation of average values and distributions of the orientation factor $\kappa^2$ for FRET between membrane-bound chromophores, using as inputs transverse location and orientation data obtained from experiments or simulations.[87] This method was applied to the computation of $\langle\kappa^2\rangle$ estimates, which could be used for calculation of the FRET Förster radius $R_0$ (with advantage over the widely used but very seldom justified $\langle\kappa^2\rangle$ = 2/3 assumption) in common membrane FRET donor–acceptor pairs. Among the latter, the values $\langle\kappa^2\rangle$(NBD/NBD) = 0.66 ± 0.03 and $\langle\kappa^2\rangle$(NBD/rhodamine B PE) = 0.56 ± 0.02 are reported in Table 1 of that reference. These values were actually calculated using parameters obtained in our simulations of NBD-PC, and as such should be used primarily with these analogues. For NBD-diC$_n$PE, one should now instead use values based on the short axis orientation distributions reported in the present work. Replacement of the orientation parameters $\theta_{max,NBD}$ (maximal value of the angular distribution of the transition dipole) and $\sigma_{NBD}$ (input standard deviation for the intended distribution of $\cos(\theta_{max,NBD})$) with 70° and 0.5, respectively (to generate wide $\theta_{max,NBD}$ distributions centred around 70°, similar to those of Fig. 5B), together with a slight refinement of the transverse location to 1.40 nm, results in $\langle\kappa^2\rangle$(NBD-diC$_n$PE/NBD-diC$_n$PE) = 0.814 ± 0.002 and $\langle\kappa^2\rangle$(NBD-diC$_n$PE/rhodamine B PE) = 0.917 ± 0.004 (standard deviations correspond to fluctuations in 10 replicate simulations, each involving $10^7$ donor–acceptor pairs). Compared with NBD-PC, the higher values reflect the increased proximity of the transition dipole of NBD to the bilayer plane (a pure isotropic in-plane distribution would produce $\langle\kappa^2\rangle$ = 5/4[88]).

# Concluding remarks

In this work, an MD study of POPC bilayers, with inserted NBD-diC$_n$PE fluorescent probes of varying acyl chain length $n$, was carried out. Like other previously studied NBD lipid probes, the transverse distribution of the fluorophore of NBD-diC$_n$PE is wide, spanning huge variations in water penetration, local dielectric constant, and hence, probe-perceived polarity. Given the sensitivity of NBD fluorescence decay to solvent polarity (becoming very fast in water), one can safely attribute the complexity of the time-resolved fluorescence emission from membrane-inserted NBD probes to this environmental heterogeneity. Attachment of the fluorophore to a PE head group does not alter its preferred location (near the glycerol backbone/carbonyl region), but changes its orientation and the pattern of H-bond interactions between the NBD amino group donor and lipid acceptors, which in turn are probable causes for differences in the decay parameters of the two most common NBD phospholipid probes (NBD-diC$_n$PE and NBD-PC), and also affect the values of orientation factor averages relevant to FRET involving NBD-diC$_n$PE as a donor and/or an acceptor.

Comparing along the series, very slight (within the statistical uncertainty) but consistent changes are apparent in the area/POPC molecule (decreasing), bilayer thickness (increasing) and acyl chain order parameters (increasing) when the acyl chain length of the probe is augmented. In most derivatives this ordering effect is not felt in the nearest neighbours surrounding each probe, but mostly in the second-nearest and more distant neighbours. This is observed because, even though the probe disorders nearby POPC acyl chains in these systems, this effect is superseded by ordering induced by binding of $Na^+$ ions to carbonyl/glycerol lipid atoms. The exception to this pattern is NBD-diC$_{16}$PE, which induces a significant ordering of nearby POPC chains. This probe in particular displays perfect matching with POPC acyl chains, and its packing and ordering abilities may be related to the reported favourable partition into liquid ordered phases of NBD-diC$_{16}$PE and NBD-diC$_{18}$PE (the latter should be better accommodated inside domains enriched in longer, predominantly saturated chains such as those of sphingomyelin inside lipid rafts). However, full clarification of this matter will involve additional work, focused on cholesterol-containing liquid ordered bilayers, and including calculation of the changes in solute free energy across the bilayer (as recently done by us for the NBD-C$_n$ series in POPC[89]).

# Acknowledgements

H. A. L. F. acknowledges funding by Fundação para a Ciência e Tecnologia (FCT), Portugal, grant reference SFRH/BD/65375/2009. L. M. S. L., H. A. L. F. and M. J. M. acknowledge additional funding by FCT, project reference UID/QUI/00313/2013. The authors acknowledge the Laboratory for Advanced Computing at University of Coimbra for computing resources.

# Notes and references

1 R. B. Gennis, *Biomembranes: molecular structure and function*, Springer-Verlag, New York, 1989.

2 M. Edidin, *Nat. Rev. Mol. Cell Biol.*, 2003, **4**, 414–418.
3 M. Luckey, *Membrane structural biology: with biochemical and biophysical foundations*, Cambridge, New York, 2008.
4 P. Fagone and S. Jackowski, *J. Lipid Res.*, 2009, **50**, S311–S316.
5 *Fluorescent Methods to Study Biological Membranes*, ed. Y. Mély and G. Duportail, Springer, Berlin, 2013.
6 A. Chattopadhyay, *Chem. Phys. Lipids*, 1990, **53**, 1–15.
7 S. Mazères, V. Schram, J. F. Tocanne and A. Lopez, *Biophys. J.*, 1996, **71**, 327–335.
8 S. Mukherjee, H. Raghuraman, S. Dasgupta and A. Chattopadhyay, *Chem. Phys. Lipids*, 2004, **127**, 91–101.
9 A. Chattopadhyay and E. London, *Biochemistry*, 1987, **26**, 39–45.
10 F. S. Abrams and E. London, *Biochemistry*, 1993, **32**, 10826–10831.
11 D. Huster, P. Müller, K. Arnold and A. Herrmann, *Biophys. J.*, 2001, **80**, 822–831.
12 D. Huster, P. Müller, K. Arnold and A. Herrmann, *Eur. Biophys. J.*, 2003, **32**, 47–54.
13 L. M. S. Loura and J. P. Prates Ramalho, *Biochim. Biophys. Acta*, 2007, **1768**, 467–478.
14 L. M. S. Loura, F. Fernandes, A. C. Fernandes AC and J. P. Prates Ramalho, *Biochim. Biophys. Acta*, 2008, **1778**, 491–501.
15 H. Scheidt, P. Müller, A. Herrmann and D. Huster, *J. Biol. Chem.*, 2003, **278**, 45563–45569.
16 J. R. Robalo, J. P. Prates Ramalho and L. M. S. Loura, *J. Phys. Chem. B*, 2013, **117**, 13731–13742.
17 M. S. C. Abreu, M. J. Moreno and W. L. C. Vaz, *Biophys. J.*, 2004, **87**, 353–365.
18 L. M. B. B. Estronca, M. J. Moreno, J. A. N. Laranjinha, L. M. Almeida and W. L. C. Vaz, *Biophys. J.*, 2005, **88**, 557–565.
19 M. J. Moreno, L. M. B. B. Estronca and W. L. C. Vaz, *Biophys. J.*, 2006, **91**, 873–881.
20 L. M. S. Loura, A. Fedorov and M. Prieto, *J. Phys. Chem. B*, 2000, **104**, 6920–6931.
21 U. Marx, G. Lassmann, H. G. Holzhütter, D. Wüstner, P. Müller, A. Höhlig, J. Kubelt and A. Herrmann, *Biophys. J.*, 2000, **78**, 2628–2640.
22 L. M. S. Loura, A. Fedorov and M. Prieto, *Biophys. J.*, 2001, **80**, 776–788.
23 C. Leidy, W. F. Wolkers, K. Jørgensen, O. G. Mouritsen and J. H. Crowe, *Biophys. J.*, 2001, **80**, 1819–1828.
24 R. F. M. de Almeida, L. M. S. Loura, A. Fedorov and M. Prieto, *J. Mol. Biol.*, 2005, **346**, 1109–1120.
25 D. K. Struck, D. Hoekstra and R. E. Pagano, *Biochemistry*, 1981, **20**, 4093–4099.
26 L. M. S. Loura, A. Coutinho, A. Silva, A. Fedorov and M. Prieto, *J. Phys. Chem. B*, 2006, **110**, 8130–8141.
27 L. M. S. Loura, *Int. J. Mol. Sci.*, 2012, **13**, 14545–14564.
28 R. F. M. de Almeida, L. M. S. Loura, A. Fedorov and M. Prieto, *Biophys. J.*, 2001, **82**, 823–834.
29 L. C. Silva, R. F. M. de Almeida, B. M. Castro, A. Fedorov and M. Prieto, *Biophys. J.*, 2007, **92**, 502–516.
30 J. Juhasz, D. H. Davis and F. J. Sharom, *Biochem. J.*, 2010, **430**, 415–423.
31 A. S. Klymchenko and R. Kreder, *Chem. Biol.*, 2014, **21**, 97–113.
32 L. M. S. Loura and J. P. Prates Ramalho, *Molecules*, 2011, **16**, 5437–5452.
33 H. A. L. Filipe, M. J. Moreno and L. M. S. Loura, *J. Phys. Chem. B*, 2011, **115**, 10109–10119.
34 A. Kyrychenko, *Chem. Phys. Lett.*, 2010, **485**, 95–99.
35 B. Hess, C. Kutzner, D. van der Spoel and E. Lindahl, *J. Chem. Theory Comput.*, 2008, **4**, 435–447.
36 S. Pronk, S. Páll, R. Schulz, P. Larsson, P. Bjelkmar, R. Apostolov, M. R. Shirts, J. C. Smith, P. M. Kasson, D. van der Spoel, B. Hess and E. Lindahl, *Bioinformatics*, 2013, **29**, 845–854.
37 H. J. C. Berendsen, J. P. M. Postma, W. F. Van Gunsteren and J. Hermans, in *Intermolecular Forces*, ed. B. Pullman, Reidel, Dordrecht, The Netherlands, 1981, pp. 331–342.
38 O. Berger, O. Edholm and F. Jähnig, *Biophys. J.*, 1997, **72**, 2002–2013.
39 M. Bachar, P. Brunelle, D. P Tieleman and A. Rauk, *J. Phys. Chem. B*, 2004, **108**, 7170–7179.
40 http://wcm.ucalgary.ca/tieleman/downloads, accessed March 2015.
41 L. M. S. Loura, A. J. Palace Carvalho and J. P. Prates Ramalho, *THEOCHEM*, 2010, **946**, 107–112.
42 A. Chattopadhyay and E. London, *Biochim. Biophys. Acta*, 1988, **938**, 24–34.
43 B. H. Besler, K. M. Merz and P. A. Kollman, *J. Comput. Chem.*, 1990, **11**, 431–439.
44 M. W. Schmidt, K. K. Baldridge, J. A. Boatz, S. T. Elbert, M. S. Gordon, J. H. Jensen, S. Koseki, N. Matsunaga, K. A. Nguyen, S. Su, T. L. Windus, M. Dupuis and J. A. Montgomery, *J. Comput. Chem.*, 1993, **14**, 1347–1363.
45 M. S. Gordon and M. W. Schmidt, in *Theory and Applications of Computational Chemistry, the first 40 years*, ed. C. E. Dykstra, G. Frenking, K. S. Lim and G. E. Scusaria, Elsevier, Amsterdam, 2005, ch. 41, pp. 1167–1189.
46 S. Miyamoto and P. A. Kollman, *J. Comput. Chem.*, 1992, **13**, 952–962.
47 B. Hess, H. Bekker, H. J. C. Berendsen, J. G. Em and M. Fraaije, *J. Comput. Chem.*, 1997, **18**, 1463–1472.
48 H. J. C. Berendsen, J. P. M. Postma, W. F. van Gunsteren, A. DiNola and J. R. Haak, *J. Chem. Phys.*, 1984, **81**, 3684–3690.
49 G. Bussi, D. Donadio and M. Parrinello, *J. Chem. Phys.*, 2007, **126**, 014101.
50 U. Essmann, L. Perera, M. L. Berkowitz, T. Darden, H. Lee and L. G. Pedersen, *J. Chem. Phys.*, 1995, **103**, 8577–8593.
51 W. Humphrey, A. Dalke and K. Schulten, *J. Mol. Graphics*, 1996, **14**, 33–38.
52 J. Seelig, *Q. Rev. Biophys.*, 1977, **10**, 353–418.
53 D. P. Tieleman and H. J. C. Berendsen, *J. Chem. Phys.*, 1996, **105**, 4871–4880.
54 H. Flyvbjerg and H. G. Petersen, *J. Chem. Phys.*, 1989, **91**, 461–466.
55 R. M. S. Cardoso, H. A. L. Filipe, F. Gomes, N. D. Moreira, W. L. C. Vaz and M. J. Moreno, *J. Phys. Chem. B*, 2010, **114**, 16337–16346.

56 R. M. S. Cardoso, P. A. T. Martins, F. Gomes, S. Doktorovova, W. L. C. Vaz and M. J. Moreno, *J. Phys. Chem. B*, 2011, **115**, 10098–10108.
57 G. Lantzsch, H. Binder, H. Heerklotz, M. Wendling and G. Klose, *Biophys. Chem.*, 1996, **58**, 289–302.
58 B. Konig, U. Dietrich and G. Klose, *Langmuir*, 1997, **13**, 525–532.
59 N. Kučerka, S. Tristram-Nagle and J. F. Nagle, *J. Membr. Biol.*, 2005, **208**, 193–202.
60 R. A. Bockmann, A. Hac, T. Heimburg and H. Grubmüller, *Biophys. J.*, 2003, **85**, 1647–1655.
61 S. Ollila, M. T. Hyvönen and I. Vattulainen, *J. Phys. Chem. B*, 2007, **111**, 3139–3150.
62 A. Gurtovenko and I. Vattulainen, *J. Phys. Chem. B*, 2008, **112**, 1953–1962.
63 G. Lukat, J. Krüger and B. Sommer, *J. Chem. Inf. Model.*, 2013, **53**, 2908–2925.
64 Please note that the definition of the short and long axes of the NBD fluorophore in Fig. 7A of ref. 13 is mistakenly indicated as opposite of that presented in this work. Despite this error, the angular distributions of NBD in NBD-PC shown in Fig. 7B–D and their discussion in that reference are correct, and may be directly compared to those described here for NBD-di$C_n$PE.
65 A. Gurtovenko and I. Vattulainen, *J. Am. Chem. Soc.*, 2007, **129**, 5358–5359.
66 L. S. Vermeer, B. L. de Groot, V. Réat, A. Milon and J. Czaplicki, *Eur. Biophys. J.*, 2007, **36**, 919–931.
67 T. M. Ferreira, F. Coreta-Gomes, O. H. S. Ollila, M. J. Moreno, W. L. C. Vaz and D. Topgaard, *Phys. Chem. Chem. Phys.*, 2013, **15**, 1976–1989.
68 J. Seelig and N. Waespe-Šarčević, *Biochemistry*, 1978, **17**, 3310–3315.
69 G. Klose, B. Mädler, H. Schäfer and K. Schneider, *J. Phys. Chem. B*, 1999, **103**, 3022–3029.
70 H. A. Scheidt, T. Meyer, J. Nikolaus, D. J. Baek, I. Haralampiev, L. Thomas, R. Bittman, P. Müller, A. Herrmann and D. Huster, *Angew. Chem., Int. Ed.*, 2013, **52**, 12848–12851.
71 T. Meyer, D. J. Baek, R. Bittman, I. Haralampiev, P. Müller, A. Herrmann, D. Huster and H. A. Scheidt, *Chem. Phys. Lipids*, 2014, **184**, 1–6.
72 S. A. Pandit, D. Bostick and M. L. Berkowitz, *Biophys. J.*, 2003, **85**, 3120–3131.
73 J. J. López Cascales, S. D. Oliveira Costa, A. Garro and R. D. Enriz, *RSC Adv.*, 2012, **2**, 11743–11750.
74 G. Pabst, A. Hodzic, J. Štrancar, S. Danner, M. Rappolt and P. Laggner, *Biophys. J.*, 2007, **93**, 2688–2696.
75 S. K. Kandasamy and R. G. Larson, *Biochim. Biophys. Acta*, 2006, **1758**, 1274–1284.
76 M. J. Skaug, M. L. Longo and R. Faller, *J. Phys. Chem. B*, 2009, **113**, 8758–8766.
77 T. Kochy and T. M. Bayerl, *Phys. Rev. E: Stat. Phys., Plasmas, Fluids, Relat. Interdiscip. Top.*, 1993, **47**, 2109–2116.
78 W. L. C. Vaz, R. M. Clegg and D. Hallmann, *Biochemistry*, 1985, **24**, 781–786.
79 B. Chazotte, *Cold Spring Harb. Protoc.*, 2011, DOI: 10.1101/pdb.prot5621.
80 M. J. Skaug, M. L. Longo and R. Faller, *J. Phys. Chem. B*, 2011, **115**, 8500–8505.
81 S. Mukherjee, H. Raghuraman, S. Dasgupta and A. Chattopadhyay, *Chem. Phys. Lipids*, 2004, **127**, 91–101.
82 S. Fery-Forgues, J.-P. Fayet and A. Lopez, *J. Photochem. Photobiol., A*, 1993, **70**, 229–243.
83 A. M. T. M. do Canto, P. D. Santos, J. Martins and L. M. S. Loura, *Colloids Surf., A*, 2015, DOI: 10.1016/j.colsurfa.2014.12.012.
84 A. S. Ito, A. P. Rodrigues, W. M. Pazin and M. B. Barioni, *J. Lumin.*, 2015, **158**, 153–159.
85 D. R. James and W. R. Ware, *Chem. Phys. Lett.*, 1985, **120**, 455–459.
86 P. A. Paprica, N. C. Baird and N. O. Petersen, *J. Photochem. Photobiol., A*, 1993, **70**, 51–57.
87 L. M. S. Loura, *Int. J. Mol. Sci.*, 2012, **13**, 15252–15270.
88 J. Knoester and J. E. van Himbergen, *J. Chem. Phys.*, 1984, **81**, 4380–4388.
89 H. A. L. Filipe, M. J. Moreno, T. Róg, I. Vattulainen and L. M. S. Loura, *J. Phys. Chem. B*, 2014, **118**, 3572–3581.

 